Parasites & Vectors

RESEARCH Open Access

Aedes aegypti Malpighian tubules are immunologically activated following systemic Toll activation

Sarah D. Sneed†, Sutopa B. Dwivedi†, Cameron DiGate, Shane Denecke and Michael Povelones*

Abstract

Background: Canine heartworm is a widespread and potentially fatal mosquito-borne disease caused by infections with the parasitic nematode, *Dirofilaria immitis*. We have previously shown that systemic activation of the Toll immune pathway via silencing of the negative regulator *Cactus* in *Aedes aegypti* blocks parasite development in the Malpighian tubules (MT), the mosquito renal organ. However, it was not established whether the MT were directly responding to Toll activation or were alternatively responding to upregulated proteins or other changes to the hemolymph driven by other tissues. Distinguishing these possibilities is crucial for developing more precise strategies to block *D. immitis* while potentially avoiding the fitness cost to the mosquito associated with *Cactus* silencing.

Methods: This study defines the transcriptional response of the MT and changes to the hemolymph proteome of *Ae. aegypti* after systemic Toll activation via intra-thoracic injection of double-stranded *Cactus* (ds*Cactus*) RNA.

Results: Malpighian tubules significantly increased expression of the Toll pathway target genes that significantly overlapped expression changes occurring in whole mosquitoes. A significant overlap between the transcriptional response of the MT and proteins upregulated in the hemolymph was also observed.

Conclusions: Our data show that MT are capable of RNA interference-mediated gene silencing and directly respond to ds*Cactus* treatment by upregulating targets of the canonical Toll pathway. Although not definitive, the strong correspondence between the MT transcriptional response and the hemolymph proteomic responses provides evidence that the MT may contribute to mosquito humoral immunity.

Keywords: *Aedes aegypti*, Malpighian tubules, Hemolymph, Innate immunity, Proteomics

Background

Vector-borne pathogens constitute a significant portion of the global infectious disease burden for both humans and animals [1]. Filarial nematodes transmitted by *Aedes*, *Culex* and *Anopheles* mosquitoes are responsible for a significant proportion of this burden. There are currently 863 million people at risk for lymphatic filariasis, which is caused by infection with *Wuchereria bancrofti*, *Brugia malayi* or *Brugia timori* [2, 3]. There are also millions of dogs, cats and other small mammals at risk for infection with *Dirofilaria immitis*, the causative agent of heartworm, for which canines are the definitive host [4–6]. The mosquito innate immune system is an important determinant of vector competency. Therefore, understanding how the mosquito responds to filarial infection and which tissues are possible sites of immune activation and pathogen restriction is essential. Identification of these mechanisms will ultimately lead to potential targets for novel transmission-blocking strategies. Modifying

†Sarah D. Sneed and Sutopa B. Dwivedi contributed equally

*Correspondence: mpove@vet.upenn.edu

Department of Pathobiology, School of Veterinary Medicine, University of Pennsylvania, Philadelphia, PA 19104, USA

the immune system to block an invading pathogen without imposing a direct fitness cost on the mosquito is the foundation of many translational strategies seeking to reduce vector-borne disease.

Principal cells of the Malpighian tubules (MT), the mosquito renal organ, are invaded by *D. immitis* microfilariae that are acquired in the blood meal of a female mosquito. In the principal cells of susceptible mosquitoes (such as *Ae. aegypti* "Blackeye" strain [*Ae. aegypti*^{BE}]), microfilariae develop into first instar/stage larvae (L1) and then molt twice forming infective third-instar larvae (L3) that migrate through the body cavity, reside in the head and labial sheath of the proboscis and are ultimately deposited in a drop of hemolymph on the skin of a host during blood-feeding. In the refractory strain *Ae. aegypti* "Liverpool," microfilariae invade principal cells but fail to develop to L1 [7–11], demonstrating that the MT are a critical tissue that can restrict parasite development. In a previous study in which we compared the transcriptional response of the MT during *D. immitis* infection, we found that both susceptible and refractory strains upregulate immune genes, but the magnitude of the response was significantly greater in the refractory strain [7]. Provoking strong immune activation by RNA interference (RNAi)-mediated gene silencing of the Toll pathway negative regulator *Cactus* greatly reduced the number of *D. immitis* and *B. malayi* L3 capable of emerging from susceptible mosquitoes [7, 12]. In the case of *D. immitis*, the reduction in emerging L3 could be accounted for by an increase in the number of immature larvae arrested in the MT [7].

Despite our previous work showing that *Cactus* RNAi-mediated Toll activation was sufficient to prevent the development of *D. immitis,* it was unclear whether this was the result of a MT-specific response or signals from other tissues. In the study presented here, we begin to address this question by performing messenger RNA (mRNA) sequencing of dissected MT from the susceptible *Ae. aegypti*^{BE} strain treated with double-stranded *Cactus* (ds*Cactus*) RNA and compared the response to that of whole mosquitoes, which have previously been shown to upregulate Toll pathway targets. We also performed proteomic analysis of the hemolymph to determine what proteins are upregulated following ds*Cactus* treatment. Our results suggest that in both the MT and the hemolymph, there is a robust upregulation of Toll-pathway effectors, including antimicrobial peptides (AMPs), C-type lectins (CTLs) and CLIP-serine proteases (CLIPs). We hypothesize that the MT may contribute to the systemic immune response in the mosquito by secreting factors into the hemolymph.

Methods

Mosquito rearing and maintenance

The susceptible *Ae. aegypti*^{BE} strain was provided by the National Institutes of Health/National Institute of Allergy and Infectious Diseases (NIH/NIAID) Filariasis Research Reagent Resource Center for distribution by BEI Resources, NIAID, NIH (*Aedes aegypti*, Strain Black Eye Liverpool, Eggs, NR-48921; https://www.beiresources.org/Catalog/BEIVectors/NR-48921.aspx). Mosquitoes were reared at 28 °C and a relative humidity of 75% on a 12/12-h light/dark photoperiod. Larvae were fed a 1% suspension of liver powder (MP Biomedicals, Santa Ana, CA, USA) in water and fish food (Tetra variety pellets; Tetra Werke, Melle Germany), while adults were fed 10% sucrose. Mosquitoes were housed in 20-cm^3 cages (Bugdorm) at density of $\leq$ 1000 adults per cage. Using an artificial membrane feeder, mosquitoes were fed heparinized sheep blood (HemoStat Laboratories, Dixon, CA, USA) warmed to 37 °C. All experiments were performed with adult female mosquitoes 3–7 days after eclosion.

Gene knockdown

Aedes aegypti Cactus dsRNA was silenced by RNAi using standard protocols and as previously published [7]. dsRNA made from a region of *Escherichia coli* β-galactosidase (*LacZ)* was used as a control. Fragments of *Cactus* (329 bp) and *LacZ* (541 bp) were amplified by PCR using 5' and 3' primers with overhangs containing T7 binding sites, using iProof High-Fidelity Taq (Bio-Rad Laboratories, Inc.). PCR reaction products were run on an agarose gel to check for the correct amplicon, purified using the GeneJet PCR purification kit (Thermo Fisher Scientific, Waltham, MA, USA), and 1 µg was used to generate dsRNA using a HiScribe T7 RNA synthesis kit (New England Biolabs [NEB] Ipswich, MA, USA). Reaction products were purified with the GeneJET RNA Purification Kit (Thermo Fisher Scientific), eluted using nuclease-free water and concentrated, with a SpeedVac to a final concentration of 3 µg/µl. Primers used for the PCR in 5' to 3' orientation, respectively, were Cactus Forward (CGAGTCAACAGAACCCGAGCAG) and Cactus Reverse (TGGCCCGTCAGCACCGAAAG), and LacZ Forward (AGAATCCGACGGGTTGTTACT) and LacZ Reverse (CACCACGCTCATCGATAATTT). All primers listed have a T7 binding site (TAATACGACTCACTA TAGGG) to the 5' end. Three biological replicates were performed on separate mosquito generations. For each experiment, groups of 150 mosquitoes were anaesthetized using CO_2 and injected intra-thoracically with 69 nl of dsRNA (207 ng) using a Nanoject III injector (Drummond Scientific Company, Broomall, PA, USA). Mosquitoes were recovered for 5 days under standard culture

conditions and then processed. The number of dead mosquitoes was recorded, and approximately 50 mosquitoes were used to prepare hemolymph samples for proteomics, and groups of 50 and 10 mosquitoes were used to prepare RNA samples for transcriptomics from dissected MT and intact whole mosquitoes, respectively.

RNA-sequencing and processing

Groups of 10 whole mosquitoes and 50 MT were dissected in phosphate-buffered saline, 10 at a time, and then transferred in TRIzol (Invitrogen™, Thermo Fisher Scientific) into a 1.5-ml rubber-gasketed screw-cap tube and frozen at − 80 °C. Once all samples were collected from three independent mosquito generations, total RNA was isolated following the manufacturer's protocol, resuspended in ultrapure water and frozen at - 80 °C. RNA samples were sent to Novogene (Davis, CA, USA) for RNA-sequencing (RNA-seq). Briefly, mRNA was isolated using oligo d(T) magnetic beads, and complementary DNA (cDNA) libraries were generated using random hexamers. Unstranded libraries of 150-bp paired-end reads were then sequenced using the NovaSeq 6000 platform (Illumina, Inc., San Diego, CA, USA) which generated FastQ files that were used for downstream analysis. The FastQ files were first filtered for quality using the "fastP" (version 0.20.1) program with the "–detect_adapter_for_pe" argument and implementing a minimum read length of 20 bp [13]. Trimmed reads were then mapped to the *Ae. aegypti* LVP_AGWG reference genome version 53 obtained from VectorBase/VEuPathDB [14, 15], using the HiSAT2 read mapper (version 2.2.0) [16]. Aligned reads were quantified using the featureCounts program [17], with the *Ae. aegypti* Gene Transfer Format file corresponding to genome version 53 (VectorBase). Differential expression analysis was then performed using the edgeR package (version 3.38.2) [18], using a false discovery rate (FDR) threshold of $q < 0.05$ and a fold-change threshold of $\log_2$ fold change ($\log_2$FC) > 2. Raw counts were subsequently normalized by conversion into transcripts per million (TPM). Gene Set Enrichment Analysis (GSEA) was performed using the Fast Gene Set Enrichment Analysis (FGSEA) tool in R (version 1.22.0) [19] and using various gene sets derived from other studies as inputs (Additional file 1: Table S1) [20–23].

Hemolymph sample preparation for western blot and proteomic analyses

Samples of hemolymph were prepared according to our standard proboscis-clipping method [24]. Briefly, groups of approximately 50 mosquitoes were initially anesthetized with CO_2 and then transferred to ice. They were then aligned into rows, ventral side up, and the proboscis cut with fine scissors at the midpoint. Gentle, even pressure was applied to the thorax to extract a drop of hemolymph, which was collected into 5-µl of non-reducing sodium dodecyl sulfate-polyacrylamide gel electrophoresis (SDS-PAGE) sample buffer (Pierce Biotechnology Inc., Thermo Fischer Scientific); approximately 15 mosquitoes were collected at a time and the sample was then transferred to a 1.5-ml protein LoBind tube (Eppendorf, Hamburg, Germany). The sample was supplemented with additional 2× sample buffer to a concentration of 1 mosquito/µl and stored at − 80 °C.

Liquid chromatography–tandom mass spectrometry analyses and data processing

Hemolymph samples were processed for liquid chromatography–tandem mass spectrometry (LC–MS/MS) as a single broad band of an SDS-PAGE gel. Each sample band was excised, de-stained using acetonitrile and then incubated with 10 mM dithiothreitol (GE HealthCare, Chicago, IL, USA) at 30 °C for 1 h. Subsequently, iodoacetamide solution (GE HealthCare) was added to a final concentration of 40 mM, and the reaction was allowed to proceed at room temperature in the dark for 30 min. The solution was incubated with trypsin (Promega, Madison, WI, USA) in a 1:50 (w/w, enzyme/protein) ratio at 37 °C for 18 h. The resulting peptides were desalted with a C-18 macro spin column (Harvard Apparatus, Holliston, MA, USA) and then vacuum dried.

LC–MS/MS analysis was performed by the Proteomics and Metabolomics Facility at the Wistar Institute using a Q Exactive Plus or Q Exactive HF mass spectrometer (Thermo Fisher Scientific) coupled with a NanoACQUITY UPLC system (Waters Corp., Milford, MA, USA). The peptide samples were injected onto a UPLC Symmetry trap column (180 µm i.d. × 2 cm, packed with 5-µm C18 resin; Waters Corp.). Tryptic peptides were separated by reversed-phase high-performance liquid chromatography on a BEH C18 nanocapillary analytical column (75 µm i.d. × 25 cm, 1.7-µm particle size; Waters Corp.) using a gradient time of 95 min, with the gradient formed by solvent A (0.1% formic acid in water) and solvent B (0.1% formic acid in acetonitrile). Eluted peptides were analyzed by the mass spectrometer set to repetitively scan m/z from 400 to 2000 in positive ion mode. The full MS scan was collected at 70,000 QE Plus or 60,000 QE HF resolution followed by data-dependent MS/MS scans at 17,500 QE Plus or 15,000 QE HF resolution on the 20 most abundant ions exceeding a minimum threshold of 10,000. Peptide match was set as preferred, exclude isotopes option and charge-state screening were enabled to reject unassigned and single charged ions.

Raw data were processed using MaxQuant (version 1.6.17.0) and the peptide search engine Andromeda.

Using *Ae. aegypti* LVP version 52 (14,979 sequences) as a reference sequence, contaminants were filtered out and peptide sequence assignments were identified using the following parameters: precursor ion mass tolerance of 20 parts per million, and a fragment ion mass tolerance of 10 Da. Peptides were searched using fully tryptic cleavage constraints, and up to two internal cleavage sites were allowed for tryptic digestion. Fixed modifications consisted of carbamidomethylation of cysteine. Variable modifications considered were oxidation of methionine, protein N-terminal acetylation and asparagine deamidation. All protein identifications reported were identified by MaxQuant with a false positive error rate of < 1%. Results from MaxQuant were imported into Perseus software (version 1.6.8; Proteome Software, Portland, OR, USA) for curation, label-free quantification analysis and visualization. Data of all technical replicates were $\log_2$-transformed and normalized by subtracting the column median. FDRs were obtained using Target Decoy PSM selecting identifications with a *P*-value $\leq$ 0.05. For differential proteins analysis, the two-tailed t-test and Benjamini Hochberg validation ($P < 0.05$ and $\log_2$FC change > 1.5) were performed in Perseus. Protein set enrichment analysis of differentially expressed proteins was performed using R Bioconductor "fgsea" package (v1.22.0). Target proteins with enrichment scores > 70% and adjusted *P*-values < 0.05 were considered for further analysis.

Label-free quantitation to determine differential protein expression

Label-free quantitation (LFQ) is an MS1 quantitation approach based on peptide mass, intensity and retention time. LFQ data were filtered according to the following criteria: (i) proteins were identified in at least two replicates per group; (ii) at least one unique peptide per protein was identified; and (iii) the peptide FDR did not exceed 1%. Significance levels were statistically analyzed using a two-tailed t-test. Proteins were considered differentially expressed between control and ds*Cactus*-treated mosquitoes if there were both a *P*-value < 0.05 and a fold change $\geq$ 1.5 (ds*Cactus*/ds*LacZ*).

Data analysis and availability

Enrichment in overlapping gene sets was performed using an online tool to compare gene enrichment (http://www.nemates.org/MA/progs/overlap_stats.html) based on Fisher's exact test. Survival comparison of *Cactus* knockdown (KD) versus control (ds*LacZ*) was accomplished using Fisher's test. All other comparisons were performed internally using the appropriate statistical packages (e.g. edgeR). Our data meet all the standards regarding the Minimum Information About a Proteomics Experiment (MIAPE) specification, and data have been deposited to the ProteomeXchange Consortium (http://www.proteomexchange.org) via the PRIDE partner repository [25]. Gene identifiers described in this manuscript are: LRIM1, AAEL012086; APL1/LRIM2, AAEL024406; TEP20, AAEL001794; Cactus, AAEL000709.

Results

Knockdown of *Cactus* triggers a Toll-like immune response in MT

To characterize the MT transcriptional response of Toll-pathway activation in *Ae. aegypti*^{BE}, we injected groups of mosquitoes with ds*Cactus* and collected RNA from both whole insects and dissected MT after 5 days. We additionally collected protein samples from the hemolymph (Fig. 1a). Prior to dissection, we observed a significant decrease in mosquito survival to day 5 in the ds*Cactus*-treated group compared to the ds*LacZ*-treated control (Fig. 1b). This was not unexpected, as *Cactus* silencing has been previously reported to incur a fitness cost [7, 26, 27].

We performed mRNA-seq comparing dissected MT from ds*Cactus*- and ds*LacZ*-treated mosquitoes as well as whole mosquitoes (Fig. 1a). In total, 296,996,140 reads (average 24,749,678 per sample) were generated over a total of 12 samples (3 biological replicates each for 2 tissue types with 2 KD conditions) (Additional file 2: Table S2). In all samples > 90% of reads mapped to the genome and an average of 75% mapped onto annotated genes. Global variation among our samples was estimated through principal component analysis (PCA), and clustering of samples from the same biological conditions suggested strong repeatability between replicates. Differences between the MT and whole-body samples were largely based on the first principal component, which represented 67.8% of variation, while differences between *Cactus* KD and control samples encompassed an additional 15.5% of variation (Fig. 2a).

Differential expression analysis was performed between ds*Cactus* and ds*LacZ* transcriptomic datasets for both the MT and the whole mosquito bodies, yielding a total of 789 differentially expressed genes (DEG) across the two comparisons (Additional file 3: Table S3). A significant overlap existed between the DEG sets of the MT and whole bodies (Fig. 2b; representation factor: 24.2; $P < 9.045e\text{-}89$). Interestingly, the vast majority of DEG in the ds*Cactus* MT were significantly upregulated (243 genes) while fewer were downregulated (31 genes). In contrast, the whole body had a comparatively larger number of downregulated (343) versus upregulated (153) genes (Additional file 3: Table S3; Fig. 2c). This result suggests that treatment with ds*Cactus* drives a physiological

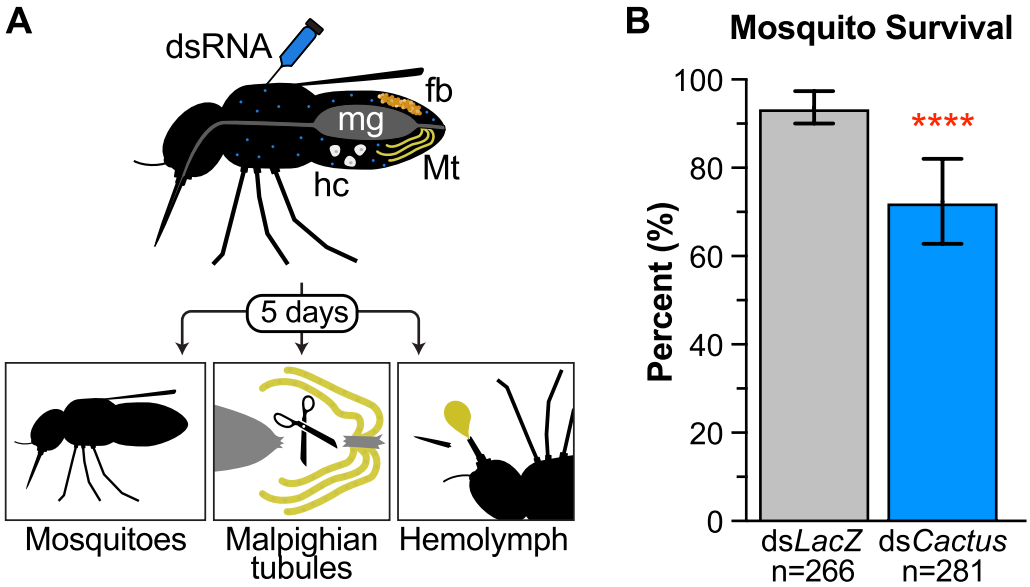

Fig. 1 Experimental overview. **a** The workflow of our experimental setup is illustrated with some mosquito tissues labeled: midgut (mg), fat body (fb), hemocytes (hc) and Malpighian tubules (Mt). Double-stranded RNA (dsRNA) targeting the *Cactus* gene was injected into the hemocoel and 5 days later RNA sequencing was performed on whole mosquitoes and dissected Malpighian tubules and proteomics was performed on the hemolymph. **b** The fitness cost of ds*Cactus* treatment was estimated by scoring survival after 5 days. Significantly more individuals from the ds*Cactus* treatment (blue) died compared to the ds*LacZ* control (gray). Asterisks indicate a Fishers exact test **P** < 0.0001. *Cactus*, Negative regulator of the Toll immune pathway in *Aedes aegypti*; *LacZ*, *Escherichia coli* β-galactosidase gene

program of increased transcriptional activity in the MT that is proportionally "more activating," or polarizing, than the transcriptional programs activated in the whole body in which the numbers of upregulated and downregulated genes are more similar.

Preceding formal analysis, several interesting transcripts stood out among those genes differentially expressed in the MT. The genes AAEL026300 and AAEL017380 showed extraordinarily high levels of abundance (>100 transcripts per million [TPM]) in *dsCactus* tubules while being almost completely absent in control tubules, showing fold changes of an order of magnitude higher than those of any other genes in this study. Both genes encode small (approx. 100 amino acids [aa]), glycine-rich secreted proteins characteristic of glycine-rich antimicrobial peptides characterized in other arthropods [28–32]. Among the 31 genes downregulated in *dsCactus* MT, three were leucine-rich immune protein family members (LRIMs) and two were prophenoloxidases (PPOs) (Additional file 3: Table S3). The *Cactus* gene itself was not differentially expressed in any sample, but this observation agrees with previous studies which have shown that genetic KD of *Cactus* occurs on short time scales, within the first 6–12 h post-injection, with phenotypes persisting far longer [7, 33, 34].

To elucidate relevant relationships within the genetic response to Toll activation, we performed GSEA, which maps user-provided gene lists onto our MT transcriptomic data ordered by fold change. Certain gene families with known essential roles in immunity, such as CLIPs, CTLs, AMPs and serpins (SRPNs) were significantly enriched in the genes upregulated in response to ds*Cactus* treatment (Fig. 3; Additional file 4: Table S4). Interestingly, PPOs, another immunity-associated gene family, showed the opposite association and were significantly enriched in the control (i.e. the genes were downregulated in response to ds*Cactus* treatment). Subunits of the vacuolar-type ATPase (vATPase) pump were also checked given the key role of this protein in epithelial physiology [35]; these genes were also significantly downregulated in *dsCactus*-treated MT (Additional file 4: Table S4). We additionally considered published transcriptomic datasets reflecting genes upregulated during *B. malayi* [20], *D. immitis* [7], and *Wolbachia* [21] infection, observing that genes that were upregulated during infection were enriched in genes upregulated during ds*Cactus* treatment (Additional file 9: Figure S1). Lastly, we observed significant correlation between genes upregulated following Toll activation via *dsCactus* treatment and activation of this pathway driven by transgenic overexpression of REL1 and REL2, two transcription factors which activate the Toll pathway [23] (Additional file 9: Figure S1). Collectively, these data suggest that in response to *dsCactus*-treatment, the MT activate canonical transcriptional

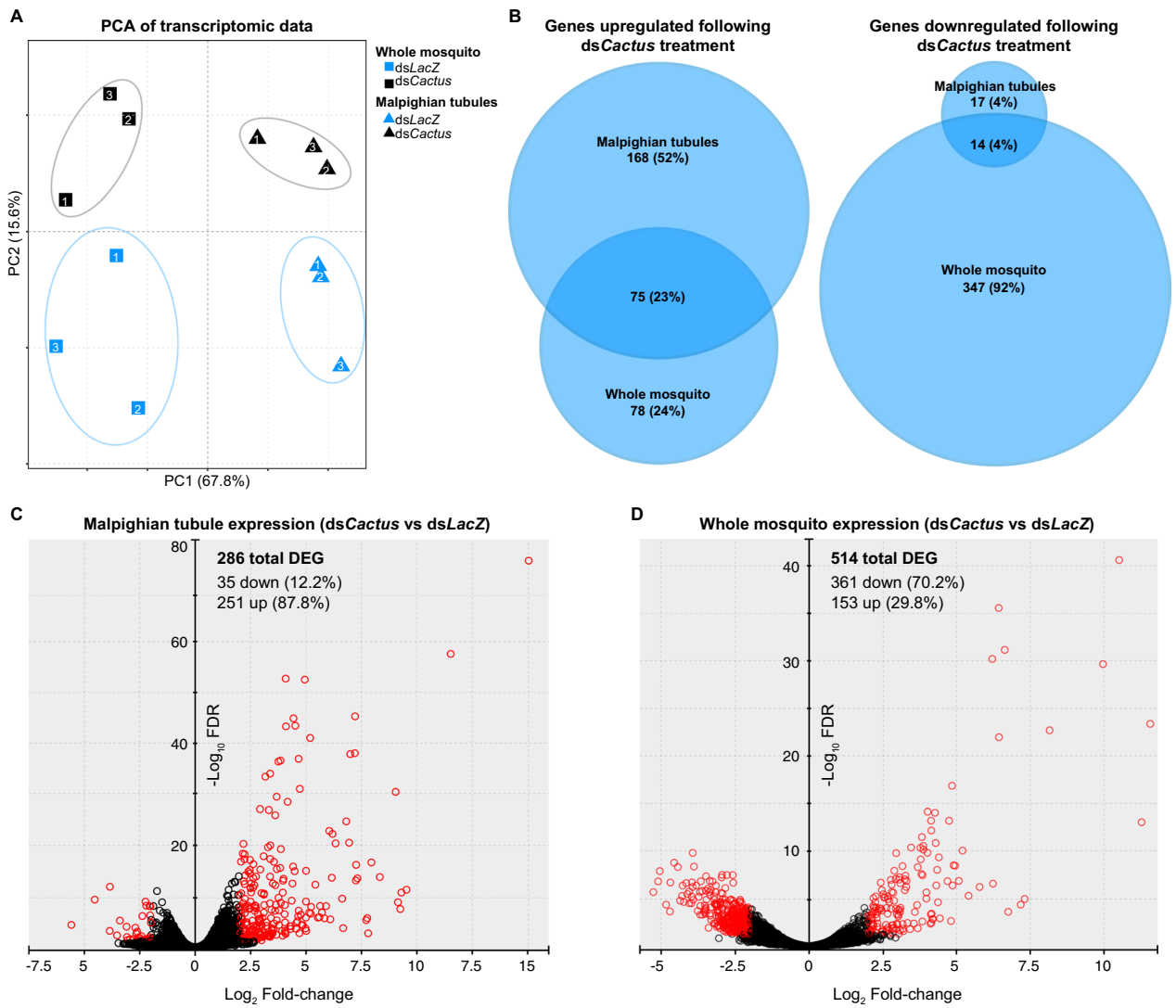

Fig. 2 Comparisons of transcriptional responses of dissected Malpighian tubules and whole mosquitoes following Toll activation. **a** PCA of RNA-sequencing of whole mosquitoes (squares) and dissected Malpighian tubules (triangles) from both ds*LacZ* (blue) and ds*Cactus* (black) treatments was visualized for global variation. Numbers indicate biological replicates. **b** Differentially expressed genes between ds*Cactus* and ds*LacZ* treatments were compared between whole bodies and Malpighian tubule-specific transcriptomes. **c**, **d** Volcano plots were made to visualize the variation in gene expression comparing ds*LacZ* versus ds*Cactus* in the Malpighian tubules (**c**) or in whole mosquitoes (**d**). Red symbols indicate genes that were significantly differentially expressed. DEG, Differentially expressed genes; PC, principal component; PCA, principal component analysis

signatures of immune activation that closely align with known transcriptional responses to infection.

Comparing the hemolymph proteome of control mosquitoes and ds*Cactus*-treated mosquitoes using high-resolution LC–MS/MS

Mass spectrometry-based proteomic analysis of hemolymph extracted from control and ds*Cactus*-treated mosquitoes revealed a total of 1319 proteins corresponding to 14,018 peptides. The complete list of peptides and their corresponding protein identification is provided in the Additional file 5: Table S5 and Additional file 6: Table S6. This is the first comprehensive hemolymph proteomic profiling of adult *Ae. aegypti* mosquitoes using nano-LC coupled to high-resolution MS. We performed LFQ analysis to identify differentially expressed hemolymph proteins between control and ds*Cactus*-treated mosquitoes. Among the hemolymph samples, approximately 64% of the variability in the data is likely related to treatment with ds*Cactus*, as represented by PCA (Fig. 4a). The

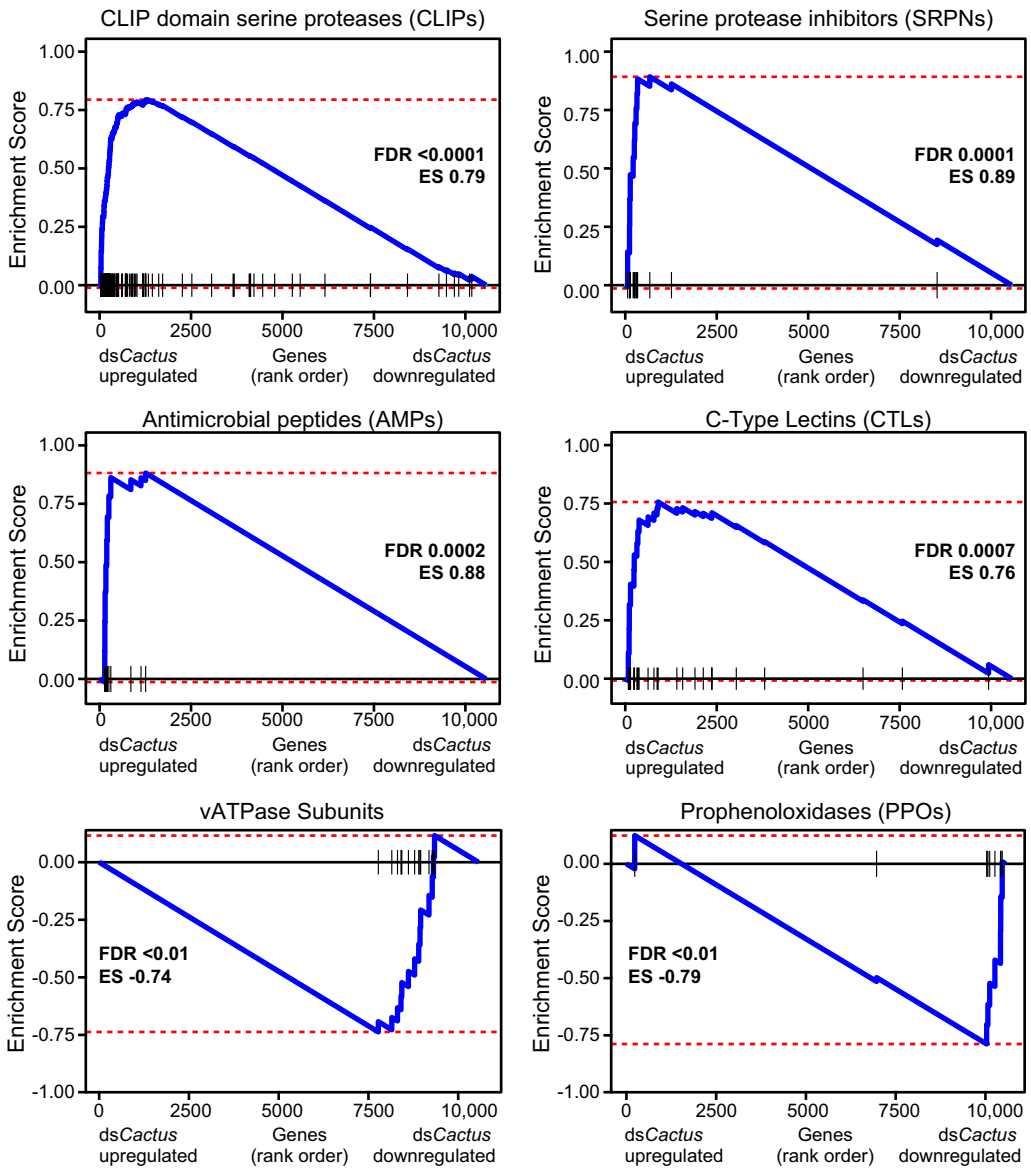

Fig. 3 Gene set enrichment analysis (GSEA) of Malpighian tubule transcriptional responses to Toll activation. GSEA was performed with six manually curated gene sets which showed significant associations in our Malpighian tubule transcriptomic comparisons. Each panel represents the association of one gene set (CLIPs, SRPNs, AMPs, CTLs, vATPases and PPOs) where the *y*-axis shows the ES, and the *x*-axis shows the $\log_2$FC rank of all genes detected in the transcriptome. Black ticks represent where genes in the respective gene list fall on the continuum of ranked genes. ES and the corrected *P*-value (FDR) for each gene set are shown. ES scores indicate genes enriched in those that are upregulated (positive ES) or downregulated (negative ES) following ds*Cactus* treatment. Full statistical description of all lists can be found in Additional file 5: Table S5. ES, Enrichment score; FDR, false discovery rate

Pearson correlation coefficients among the replicates fall within the range of 0.85–0.99, showing a close association between the replicates and suggesting high repeatability (Additional file 10: Figure S2).

To determine differentially expressed proteins between the hemolymph proteomes of control and *dsCactus*-treated mosquitoes, the normalized LFQ intensities of the identified peptides between the two experimental groups were compared. The filtered analysis led to the identification of 277 significantly upregulated and 226 significantly downregulated proteins (Additional file 7: Table S7). Protein set enrichment analysis (PSEA) using fold-change values from this analysis showed an enrichment of CLIPs, SRPNs, CTLs and other proteases, indicating the

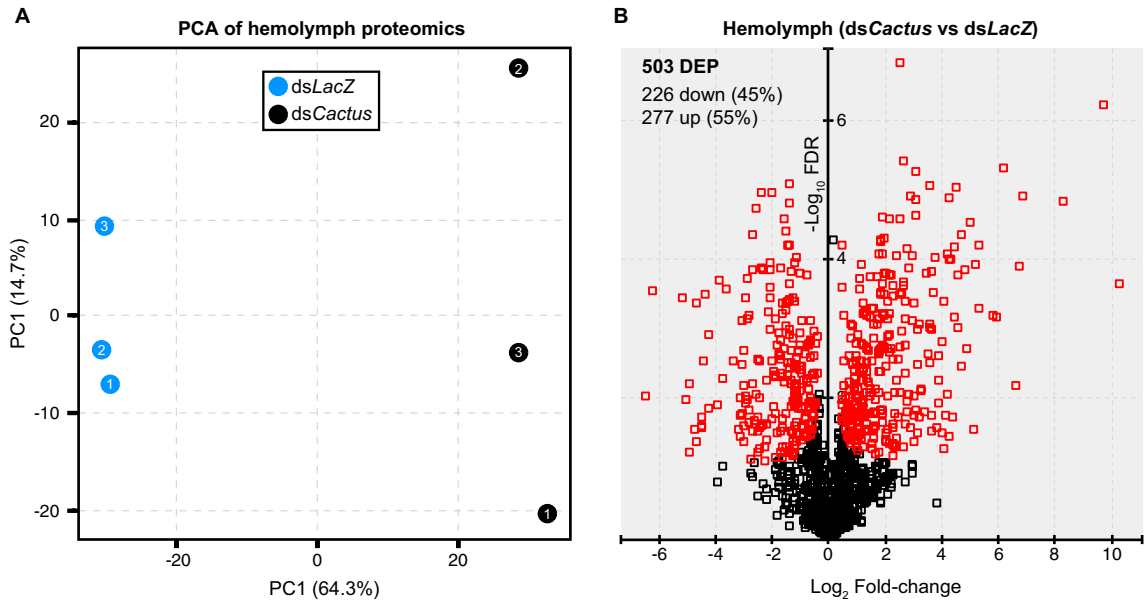

Fig. 4 Proteomic analysis of hemolymph following Toll activation. **a** PCA of all six hemolymph samples to show global variation; clustering along the first PC was observed between ds*LacZ* (blue circles) and ds*Cactus* (black circles) treatments. **b** A volcano plot was generated to estimate protein level changes among proteins identified. Red symbols indicate significantly DEP. DEP, Differentially expressed proteins

possibility of downstream melanization effector mechanisms in the hemolymph of *dsCactus*-treated mosquitoes (Additional file 11: Figure S3; Additional file 4: Table S4). Interestingly, the enrichment of CLIPs, which includes one of the most highly enriched proteins, AAEL022822, along with the increased abundance of thioester-containing protein 20 (TEP20) in the hemolymph suggests the possible accumulation of putative complement pathway components following *dsCactus* treatment. This pathway has not yet been characterized in *Ae. aegypti*, but it plays a prominent role in anti-plasmodial, anti-bacterial and anti-fungal immunity in *An. gambiae* [24, 33, 36–40]. Taken together, our data suggest that *dsCactus* treatment increases expression of proteins involved in mosquito immunity with specific enrichment of proteins involved in the Toll and putative complement pathways.

Determining the potential for a MT-specific contribution to systemic humoral immunity

Lastly, we tested the hypothesis of whether the hemolymph proteins upregulated in the *dsCactus* treatment might have an origin in the MT. Using GSEA, we observed that proteins significantly increased in the *dsCactus* hemolymph tended to be similarly enriched in the *dsCactus* MT RNA-seq dataset (Fig. 5a). We then identified 168 transcripts which were significantly upregulated by *dsCactus* treatment specifically in the MT but not in the whole body (Fig. 2b). When this list was intersected with hemolymph proteins upregulated by *dsCactus* treatment (Fig. 5b), we found a statistically significant overlap of 39 transcripts/proteins (representation factor: 10.0; $P < 1.868e\text{-}28$ for tubules). This group contained several putatively secreted Toll- and complement-related genes, such as several CLIPs, SRPN3 and TEP20 (Additional file 8: Table S8). While this does not definitively confirm that these proteins are secreted from the MT into the hemolymph following *dsCactus* treatment, we suggest this as a hypothesis.

Discussion

Our study demonstrates the direct transcriptional response of MT to *Cactus* systemic silencing and their capacity to broadly upregulate Toll pathway target genes in *Ae. aegypti*. Extensive work in *Drosophila* and different mosquito species has shown that hyperactivation of Toll signaling using a variety of approaches results in increased immune activation and refractoriness to immune challenge [7, 23, 26, 27, 33, 34, 41–43]. Studies in *Ae. aegypti* have shown that *dsCactus* treatment drives constitutive Toll signaling, immune activation and increased refractoriness to viral [44], fungal [41] and filarial nematode infections [7]. In *Anopheles gambiae*, activation of Toll signaling mediated by *dsCactus* treatment resulted in increased basal expression of TEP1 and LRIM1, immune genes that inhibit development of *Plasmodium*, resulting in a lower burden of parasite infection [33]. Similar studies using transgenic strains of *Ae. aegypti* overexpressing Rel1, the NF-κB transcription

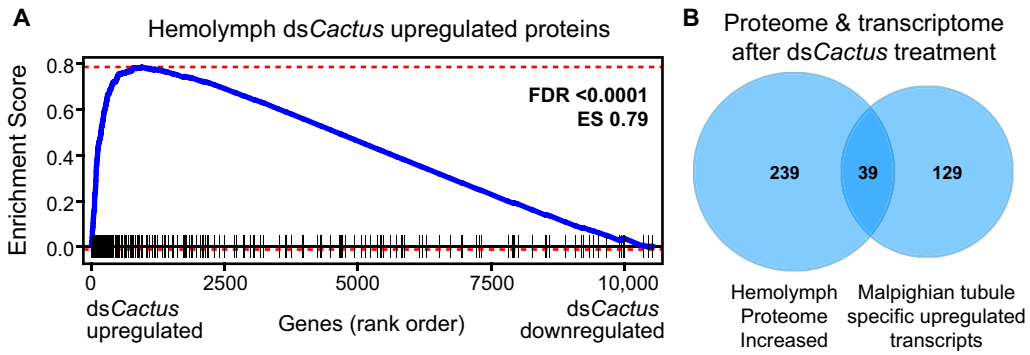

Fig. 5 Comparison of Malpighian tubule transcriptomic and hemolymph proteomic responses following Toll activation. **a** GSEA was performed on the Malpighian tubule RNA sequencing using a gene set consisting of proteins that were significantly upregulated in the hemolymph proteomics. The *y*-axis shows the ES, and the *x*-axis shows the $\log_2$FC rank of all genes detected in the Malpighian tubule transcriptome. Black ticks represent where proteins in the hemolymph-upregulated proteome gene list fall on the continuum of ranked genes. ES and the corrected *P*-value (FDR) for this analysis are shown. **b** Among the 168 genes that were significantly upregulated only in the Malpighian tubules upon ds*Cactus* treatment, 39 were also upregulated in the hemolymph proteome

factor activated downstream of Toll signaling, showed increased expression of immune genes in the absence of a pathogenic challenge [41]. The significant degree of correlation between other transcriptomes profiled during Toll activation (e.g. REL1 overexpression; infection etc.) and our dataset (Additional file 4: Table S4) confirm earlier findings that silencing of the *Cactus* gene activates the Toll pathway.

This study extends our current understanding of Toll pathway signaling by demonstrating the ability of the MT to undergo a Toll-based immune response. Our previous transcriptomic studies comparing mosquitoes susceptible and refractory to the filarial nematode *D. immitis* suggested that Toll pathway activation was sufficient to block the worm development within the tubule [7]. Correlation of the genes upregulated in the *dsCactus*-treatment samples between the MT and whole body (Fig. 2b) along with the specific upregulation of canonical Toll targets such as CTLs, CLIPs, SRPNs and PPOs in the MT (Fig. 3) strongly suggests that the MT themselves generate immune factors for pathogen defense. Interestingly, subunits of the vATPase were also downregulated following *dsCactus* treatment (Fig. 3). vATPase is a proton (H^+) pump that has been shown in *Ae. aegypti* to be responsible for the bulk of MT transepithelial secretion of KCl and NaCl. In the MT, vATPase is located in the apical brush border membrane of principal cells, and it is responsible for mediating a substantial part of post-blood meal diuresis. It was previously shown that vATPases were globally downregulated in *Aedes albopictus* MT following blood-feeding [45]. To date, there has been no evidence in mosquitoes of a direct link between vATPase expression and immunity. However, work in *Drosophila* suggests there is an important connection between physiological desiccation stress (metabolism) and immunity [46–49], so it stands a similar pathway may be at work in mosquitoes although further studies are needed to confirm this relationship.

Even more intriguing is the possibility that the MT play a more systemic role in Toll-based immunity. The relative contribution of the MT to the immune protein milieu in the hemolymph of mosquitoes has not been defined and we only sought to begin to explore this hypothesis in this study. We found a subset of genes which were enriched during Toll activation specifically in the MT that encoded proteins that were also significantly increased in the hemolymph under the same conditions (Additional file 8: Table S8). This suggests the possibility that such proteins are derived from the MT. There is precedent for a significant systemic immune contribution from the MT in *Drosophila* as antibacterial immunity develops in larvae only after development of the MT [50]. The MT are also strictly controlled by neuroendocrine factors, and in adult flies suffering from desiccation stress, ecdysone is locally produced in MT to increase the expression of immune genes and increase host defense [46]. Although the numbers are small, sessile hemocytes are present attached to the MT [51]. Additionally, blocking the MT immune response immunocompromises flies even when the fat body is intact, indicating that the contribution of the MT is systemically important [52, 53]. Future work and new genetic tools will be needed to establish the functional contribution of MT to systemic immunity in mosquitoes.

Conclusions

This work has characterized the transcriptome of MT from mosquitoes treated with *dsCactus* RNA and shown for the first time that the MT of *Ae. aegypti* can activate Toll pathway immune genes locally in response. We have also profiled the hemolymph proteins of Toll-activated mosquitoes and identified a subset of proteins present whose transcripts are differentially upregulated in the MT, suggesting possibility that the MT can contribute substantially to humoral immunity. Collectively, this work contributes to the growing body of evidence that the MT are an essential immune tissue with similarly active pathways to other known immune tissues (e.g. fat body and hemocytes), but with possibly unique physiological roles, in the mosquito immune response.

Abbreviations

AMP: Antimicrobial peptide; CLIP: CLIP-domain serine protease; CTL: C-type lectin; DEG: Differentially expressed genes; GSEA: Gene set enrichment analysis; KD: knockdown; LFQ: Label-free quantitative MS; LRIM: Leucine-rich repeat immune protein; MS: Mass spectrometry; MT: Malpighian tubules; PCA: Principal component analysis; PPO: Prophenoloxidase; PSEA: Protein set enrichment analysis; RNAi: RNA interference; SRPN: Serine protease inhibitor; TEP: Thioester-containing protein; vATPase: Vacuolar-type ATPase.

Supplementary Information

The online version contains supplementary material available at https://doi.org/10.1186/s13071-022-05567-2.

Additional file 1: Table S1. Gene lists used for the GSEA and PSEA. Column headings are gene list names and rows beneath are the VectorBase gene identifiers belong to each list. Some lists are manually curated and others are derived from previously published data sets.

Additional file 2: Table S2. Overview of Malpighian tubules and whole mosquito mRNA sequencing. An overview of the transcriptomic results is shown including total reads, mapping rates, and the percent of genes mapping to known protein encoding genes.

Additional file 3: Table S3. Differentially expressed genes from Malpighian tubules and whole mosquito mRNA sequencing. All RNA sequencing runs are shown along with their corresponding metadata. Down- and upregulated genes in MT are shown in gray and blue shading, respectively. Down- and upregulated genes in whole mosquitoes are shown in orange and green shading, respectively.

Additional file 4: Table S4. Statistical values for the transcriptomic GSEA and PSEA. Gene and protein sets enriched in MT transcriptomics and hemolymph proteomics.

Additional file 5: Table S5. Peptide-level output of the hemolymph proteomics.

Additional file 6: Table S6. Proteins detected in hemolymph proteomics with their associated metadata.

Additional file 7: Table S7. Differentially expressed proteins in hemolymph proteomics from dsCactus treated mosquitoes.

Additional file 8: Table S8. Intersection of the genes which were commonly found between: (i) genes upregulated in the ds*Cactus*-treated MT but not upregulated in the ds*Cactus*-treated whole body samples; and (ii) proteins upregulated in the ds*Cactus*-treated hemolymph proteome.

Additional file 9: Figure S1. Gene set enrichment analysis (GSEA) of Malpighian tubule transcriptional responses to Toll activation. GSEA was performed with four manually curated gene sets from previously published transcriptomic studies which showed significant associations in our Malpighian tubule transcriptomic comparisons. Each panel represents the association of one gene set where the *y*-axis shows the enrichment score (ES), and the *x*-axis shows the $\log_2$FC rank of all genes detected in the transcriptome. Black ticks represent where genes in the respective gene list fall on the continuum of ranked genes. ES and the corrected *P*-value (false discovery rate [FDR]) for each gene set shown. ES scores indicate genes are enriched in those that are upregulated (positive ES) or downregulated (negative ES) following ds*Cactus* treatment. Full statistical description of all lists can be found in Additional file: Table S5.

Additional file 10: Figure S2. Hemolymph proteomic replicates are highly correlated. Correlation analysis to demonstrate consistency between hemolymph mass spectrometry proteomic replicates. Replicate 1 (*x*-axis) is shown against replicate 3 (*y*-axis) with the correlation coefficient ρ value (0.94) shown on the graph. Below the graph are the ρ values for the other replicate comparisons, which are also highly correlated to each other.

Additional file 11: Figure S3. Protein set enrichment analysis of hemolymph response to Toll activation. The *y*-axis shows the enrichment score (ES) and the *x*-axis shows the $\log_2$FC rank of all proteins detected in the hemolymph proteome. Black ticks represent where genes of the respective proteins from curated lists fall on the continuum of ranked proteins. Full statistical description of all lists can be found in Additional file: Table S5.

Acknowledgements

We thank Abigail R. McCrea and Sarah Dysinger for technical assistance producing mosquitoes and other materials for this study.

Author contributions

SDS, SBD, SD and MP Conceived and designed the analysis. CD and MP collected the data. SDS, SBD and SD performed the analysis. SDS, SBD, SD and MP wrote the paper. All authors read and approved the final manuscript.

Funding

The funders of this work had no role in the design of the study, in the collection, analysis and interpretation of data and in the writing of the manuscript. This work was supported by NIH grants AI139060, and AI154022 and a grant from the Morris Animal Foundation D22CA-015 (MP). CD was supported by a NIH-Boehringer-Ingelheim Summer Veterinary Scholars Program and the Penn Institute for Immunology.

Availability of data and materials

All scripts used to analyze transcriptomic data were written in R or bash and are publicly available on Rpubs (https://rpubs.com/shanedenecke/Cactus_KD_analysis). Raw mRNA sequencing reads are available on NCBI Sequence Read Archive (PRJNA758024; reviewer link). Our data meet all the standards regarding the Minimum Information About a Proteomics Experiment (MIAPE), and data have been deposited to the ProteomeXchange Consortium (http://www.proteomexchange.org) via the PRIDE partner repository (px-submission #607,630).

Declarations

Ethics approval and consent to participate

Not applicable.

Consent for publication

Not applicable.

Competing interests

Not applicable.

Received: 21 August 2022 Accepted: 2 November 2022
Published online: 15 December 2022

References

1. WHO. Vector-borne diseases. 2020. https://www.who.int/news-room/fact-sheets/detail/vector-borne-diseases. Accessed 30 June 2022.
2. Taylor MJ, Hoerauf A, Bockarie M. Lymphatic filariasis and onchocerciasis. Lancet. 2010;376:1175–85. https://doi.org/10.1016/S0140-6736(10)60586-7.
3. WHO. Lymphatic filariasis. 2022. https://www.who.int/news-room/fact-sheets/detail/lymphatic-filariasis. Accessed 30 June 2022.
4. Genchi C, Solari Basano F, Marrone RV, Petruschke G. Canine and feline heartworm in Europe with special emphasis on Italy. In: Seward RL, Knight DH, editors. Proceedings of the Heartworm Symposium 1998. Batavia, IL, USA: American Heartworm Society; 1988. p. 75–82.
5. McCall JW. A parallel between experimentally induced canine and feline heartworm disease. Rome: Delfino Publisher; 1992.
6. Otto GF. Occurrence of the heartworm in unusual locations and in unusual hosts. In: Morgan HC, editor. Proceedings of the Heartworm Symposium 1974. Mooresville: VM Publishing; 1975. p. 6–13.
7. Edgerton EB, McCrea AR, Berry CT, Kwok JY, Thompson LK, Watson B, et al. Activation of mosquito immunity blocks the development of transmission-stage filarial nematodes. Proc Natl Acad Sci USA. 2020;117:3711-7. https://doi.org/10.1073/pnas.1909369117.
8. Kartman L. Factors influencing infection of the mosquito with Dirofilaria immitis (Leidy, 1856). Exp Parasitol. 1953;2:27–78. https://doi.org/10.1016/0014-4894(53)90005-8.
9. McGreevy PB, McClelland GA, Lavoipierre MM. Inheritance of susceptibility to *Dirofilaria immitis* infection in *Aedes aegypti*. Ann Trop Med Parasitol. 1974;68:97–109.
10. Nayar JK, Knight JW, Bradley TJ. Further characterization of refractoriness in *Aedes aegypti* (L.) to infection by *Dirofilaria immitis* (Leidy). Exp Parasitol. 1988;66:124–31. https://doi.org/10.1016/0014-4894(88)90057-4.
11. Sauerman DM Jr, Nayar JK. Characterization of refractoriness in *Aedes aegypti* (Diptera: Culicidae) to infection by *Dirofilaria immitis*. J Med Entomol. 1985;22:94–101. https://doi.org/10.1093/jmedent/22.1.94.
12. McCrea AR, Jimenez Castro PD, Kaplan RM, Povelones M. Activation of the Toll pathway in *Aedes aegypti* blocks the development of emerging third-stage larvae of drug-resistant *Dirofilaria immitis*. Vet Parasitol. 2020;282:109100. https://doi.org/10.1016/j.vetpar.2020.109100.
13. Chen S, Zhou Y, Chen Y, Gu J. fastp: an ultra-fast all-in-one FASTQ preprocessor. Bioinformatics. 2018;34:i884–90. https://doi.org/10.1093/bioinformatics/bty560.
14. Amos B, Aurrecoechea C, Barba M, Barreto A, Basenko EY, Bazant W, et al. VEuPathDB: the eukaryotic pathogen, vector and host bioinformatics resource center. Nucleic Acids Res. 2022;50:D898–911. https://doi.org/10.1093/nar/gkab929.
15. Giraldo-Calderon GI, Harb OS, Kelly SA, Rund SS, Roos DS, McDowell MA. VectorBase org updates: bioinformatic resources for invertebrate vectors of human pathogens and related organisms. Curr Opin Insect Sci. 2022;50:100860. https://doi.org/10.1016/j.cois.2021.11.008.
16. Kim D, Paggi JM, Park C, Bennett C, Salzberg SL. Graph-based genome alignment and genotyping with HISAT2 and HISAT-genotype. Nat Biotechnol. 2019;37:907–15. https://doi.org/10.1038/s41587-019-0201-4.
17. Liao Y, Smyth GK, Shi W. featureCounts: an efficient general purpose program for assigning sequence reads to genomic features. Bioinformatics. 2014;30:923–30. https://doi.org/10.1093/bioinformatics/btt656.
18. Robinson MD, McCarthy DJ, Smyth GK. edgeR: a Bioconductor package for differential expression analysis of digital gene expression data. Bioinformatics. 2010;26:139–40. https://doi.org/10.1093/bioinformatics/btp616.
19. Korotkevich G, Sukhov V, Budin N, Shpak B, Artyomov MN, Sergushichev A. Fast gene set enrichment analysis. Cold Spring Harbor Lab. 2016;31:608.
20. Juneja P, Ariani CV, Ho YS, Akorli J, Palmer WJ, Pain A, et al. Exome and transcriptome sequencing of Aedes aegypti identifies a locus that confers resistance to Brugia malayi and alters the immune response. PLoS Pathog. 2015;11:e1004765. https://doi.org/10.1371/journal.ppat.1004765.
21. Rances E, Ye YH, Woolfit M, McGraw EA, O'Neill SL. The relative importance of innate immune priming in *Wolbachia*-mediated dengue interference. PLoS Pathog. 2012;8:e1002548. https://doi.org/10.1371/journal.ppat.1002548.
22. Souza-Neto JA, Sim S, Dimopoulos G. An evolutionary conserved function of the JAK-STAT pathway in anti-dengue defense. Proc Natl Acad Sci USA. 2009;106:17841–6.
23. Zou Z, Souza-Neto J, Xi Z, Kokoza V, Shin SW, Dimopoulos G, et al. Transcriptome analysis of *Aedes aegypti* transgenic mosquitoes with altered immunity. PLoS Pathog. 2011;7:e1002394. https://doi.org/10.1371/journal.ppat.1002394.
24. Povelones M, Waterhouse RM, Kafatos FC, Christophides GK. Leucine-rich repeat protein complex activates mosquito complement in defense against Plasmodium parasites. Science. 2009;324:258–61. https://doi.org/10.1126/science.1171400.
25. Vizcaíno JA, Csordas A, del Toro N, Dianes José A, Griss J, Lavidas I, et al. update of the PRIDE database and its related tools. Nucleic Acids Res. 2016;2016:D447-56. https://doi.org/10.1093/nar/gkv1145.
26. Erickson SM, Xi Z, Mayhew GF, Ramirez JL, Aliota MT, Christensen BM, et al. Mosquito infection responses to developing filarial worms. PLoS Negl Trop Dis. 2009;3:e529. https://doi.org/10.1371/journal.pntd.0000529.
27. Garver LS, Dong Y, Dimopoulos G. Caspar controls resistance to Plasmodium falciparum in diverse anopheline species. PLoS Pathog. 2009;5:e1000335. https://doi.org/10.1371/journal.ppat.1000335.
28. Lee YJ, Chung TJ, Park CW, Hahn Y, Chung JH, Lee BL, et al. Structure and expression of the tenecin 3 gene in *Tenebrio molitor*. Biochem Biophys Res Commun. 1996;218:6–11. https://doi.org/10.1006/bbrc.1996.0002.
29. Iijima R, Kurata S, Natori S. Purification, characterization, and cDNA cloning of an antifungal protein from the hemolymph of *Sarcophaga peregrina* (flesh fly) larvae. J Biol Chem. 1993;268:12055–61.
30. Lorenzini DM, da Silva PI, Fogaça AC, Bulet P, Daffre S. Acanthoscurrin: a novel glycine-rich antimicrobial peptide constitutively expressed in the hemocytes of the spider *Acanthoscurria gomesiana*. Dev Comp Immunol. 2003;27:781–91. https://doi.org/10.1016/s0145-305x(03)00058-2.
31. Herbiniere J, Braquart-Varnier C, Greve P, Strub JM, Frere J, Van Dorsselaer A, et al. Armadillidin: a novel glycine-rich antibacterial peptide directed against Gram-positive bacteria in the woodlouse *Armadillidium vulgare* (Terrestrial Isopod, Crustacean). Dev Comp Immunol. 2005;29:489–99. https://doi.org/10.1016/j.dci.2004.11.001.
32. Baumann T, Kämpfer U, Schürch S, Schaller J, Largiadèr C, Nentwig W, et al. Ctenidins: antimicrobial glycine-rich peptides from the hemocytes of the spider *Cupiennius salei*. Cell Mol Life Sci. 2010;67:2787–98. https://doi.org/10.1007/s00018-010-0364-0.
33. Frolet C, Thoma M, Blandin S, Hoffmann JA, Levashina EA. Boosting NF-kappaB-dependent basal immunity of Anopheles gambiae aborts development of Plasmodium berghei. Immunity. 2006;25:677–85.
34. Rono MK, Whitten MM, Oulad-Abdelghani M, Levashina EA, Marois E. The major yolk protein vitellogenin interferes with the anti-*Plasmodium* response in the malaria mosquito *Anopheles gambiae*. PLoS Biol. 2010;8:e1000434. https://doi.org/10.1371/journal.pbio.1000434.
35. Statistical significance of the overlap between two groups of genes. http://www.nemates.org/uky/MA/progs/overlap_stats.html. Accessed 19 Aug 2022.
36. Blandin S, Shiao SH, Moita LF, Janse CJ, Waters AP, Kafatos FC, et al. Complement-like protein TEP1 is a determinant of vectorial capacity in the malaria vector *Anopheles gambiae*. Cell. 2004;116:661–70.
37. Dong Y, Aguilar R, Xi Z, Warr E, Mongin E, Dimopoulos G. *Anopheles gambiae* immune responses to human and rodent *Plasmodium* parasite species. PLoS Pathog. 2006;2:e52. https://doi.org/10.1371/journal.ppat.0020052.
38. Fraiture M, Baxter RH, Steinert S, Chelliah Y, Frolet C, Quispe-Tintaya W, et al. Two mosquito LRR proteins function as complement control factors in the TEP1-mediated killing of *Plasmodium*. Cell Host Microbe. 2009;5:273–84.
39. Levashina EA, Moita LF, Blandin S, Vriend G, Lagueux M, Kafatos FC. Conserved role of a complement-like protein in phagocytosis revealed by dsRNA knockout in cultured cells of the mosquito *Anopheles gambiae*. Cell. 2001;104:709–18.
40. Yassine H, Kamareddine L, Osta MA. The mosquito melanization response is implicated in defense against the entomopathogenic fungus *Beauveria bassiana*. PLoS Pathog. 2012;8:e1003029. https://doi.org/10.1371/journal.ppat.1003029.
41. Bian G, Shin SW, Cheon HM, Kokoza V, Raikhel AS. Transgenic alteration of toll immune pathway in the female mosquito *Aedes aegypti*. Proc Natl

Acad Sci USA. 2005;102:13568–73. https://doi.org/10.1073/pnas.0502815102.
42. Lemaitre B, Meister M, Govind S, Georgel P, Steward R, Reichhart JM, et al. Functional analysis and regulation of nuclear import of dorsal during the immune response in *Drosophila*. EMBO J. 1995;14:536–45. https://doi.org/10.1002/j.1460-2075.1995.tb07029.x.
43. Ramirez JL, Garver LS, Brayner FA, Alves LC, Rodrigues J, Molina-Cruz A, et al. The role of hemocytes in *Anopheles gambiae* antiplasmodial immunity. J Innate Immun. 2014;6:119–28. https://doi.org/10.1159/000353765.
44. Xi Z, Ramirez JL, Dimopoulos G. The *Aedes aegypti* toll pathway controls dengue virus infection. PLoS Pathog. 2008;4:e1000098. https://doi.org/10.1371/journal.ppat.1000098.
45. Esquivel CJ, Cassone BJ, Piermarini PM. Transcriptomic evidence for a dramatic functional transition of the Malpighian tubules after a blood meal in the asian tiger mosquito *Aedes albopictus*. PLoS Neglected Tropical Dis. 2014;8:e2929. https://doi.org/10.1371/journal.pntd.0002929.
46. Zheng W, Rus F, Hernandez A, Kang P, Goldman W, Silverman N, et al. Dehydration triggers ecdysone-mediated recognition-protein priming and elevated anti-bacterial immune responses in *Drosophila* Malpighian tubule renal cells. BMC Biol. 2018;16:60. https://doi.org/10.1186/s12915-018-0532-5.
47. Verma P, Tapadia MG. Early gene broad complex plays a key role in regulating the immune response triggered by ecdysone in the Malpighian tubules of *Drosophila melanogaster*. Mol Immunol. 2015;66:325–39. https://doi.org/10.1016/j.molimm.2015.03.249.
48. Rus F, Flatt T, Tong M, Aggarwal K, Okuda K, Kleino A, et al. Ecdysone triggered PGRP-LC expression controls *Drosophila* innate immunity. EMBO J. 2013;32:1626–38. https://doi.org/10.1038/emboj.2013.100.
49. Buchon N, Silverman N, Cherry S. Immunity in *Drosophila melanogaster*–from microbial recognition to whole-organism physiology. Nat Rev Immunol. 2014;14:796–810. https://doi.org/10.1038/nri3763.
50. Verma P, Tapadia MG. Immune response and anti-microbial peptides expression in Malpighian tubules of *Drosophila melanogaster* is under developmental regulation. PloS ONE. 2012;7:e40714. https://doi.org/10.1371/journal.pone.0040714.
51. King JG, Hillyer JF. Spatial and temporal in vivo analysis of circulating and sessile immune cells in mosquitoes: hemocyte mitosis following infection. BMC Biol. 2013;11:55. https://doi.org/10.1186/1741-7007-11-55.
52. Verma P, Tapadia MG. Epithelial immune response in *Drosophila* Malpighian tubules: interplay between Diap2 and ion channels. J Cell Physiol. 2014;229:1078–95. https://doi.org/10.1002/jcp.24541.
53. McGettigan J, McLennan RK, Broderick KE, Kean L, Allan AK, Cabrero P, et al. Insect renal tubules constitute a cell-autonomous immune system that protects the organism against bacterial infection. Insect Biochem Mol Biol. 2005;35:741–54. https://doi.org/10.1016/j.ibmb.2005.02.017.

Publisher's Note